# Development of RSM- and ANN-based models to predict and analyze the effects of process parameters of laser-hardened commercially pure titanium on heat input and tensile strength

**Article** *in* The International Journal of Advanced Manufacturing Technology · April 2012

DOI: 10.1007/s00170-012-4259-0

CITATIONS
22

READS
90

**3 authors**, including:

Duradundi Sawant Badkar
Ashokrao Mane Group of Institutions
**27** PUBLICATIONS **146** CITATIONS
SEE PROFILE

Buvanashekaran.G Naidu
Bharat Heavy Electricals Limited
**45** PUBLICATIONS **712** CITATIONS
SEE PROFILE

# *Development of RSM- and ANN-based models to predict and analyze the effects of process parameters of laser-hardened commercially pure titanium on heat input and tensile strength*

**Duradundi Sawant Badkar, Krishna Shankar Pandey & G. Buvanashekaran**

**The International Journal of Advanced Manufacturing Technology**

ISSN 0268-3768

Int J Adv Manuf Technol
DOI 10.1007/s00170-012-4259-0

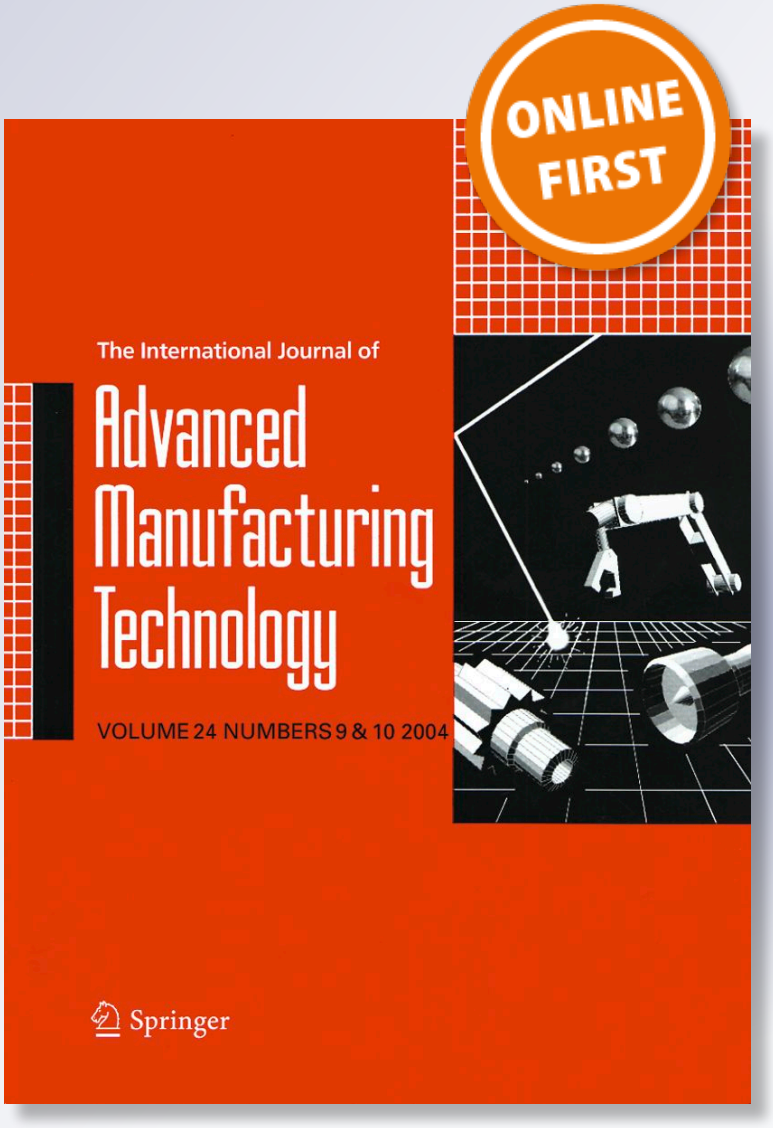


Springer

Int J Adv Manuf Technol
DOI 10.1007/s00170-012-4259-0

ORIGINAL ARTICLE

# Development of RSM- and ANN-based models to predict and analyze the effects of process parameters of laser-hardened commercially pure titanium on heat input and tensile strength

**Duradundi Sawant Badkar · Krishna Shankar Pandey · G. Buvanashekaran**

Received: 11 November 2009 / Accepted: 22 May 2012


**Abstract** Laser transformation hardening (LTH) is an innovative and advanced laser surface modification technique as compared to conventional transformation hardening processes and has been employed in aerospace, marine, chemical applications, heat exchangers, cryogenic vessels, components for chemical processing and desalination equipment, condenser tubing, airframe skin, and nonstructural components which introduces the advantageous residual stresses into the surface, improving the mechanical properties like wear, resistance to corrosion, tensile strength, and fatigue strength. In the present study, LTH of commercially pure titanium, nearer to ASTM grade 3 of chemical composition was investigated using continuous wave 2 kW, Nd: YAG laser. The effect of laser process variables such as laser power, scanning speed, and focused position was investigated using response surface methodology (RSM) and artificial neural network (ANN) keeping argon gas flow rate of 10 lpm as fixed input parameter. This paper describes the comparison of the heat input (HI) and ultimate tensile strength ($\sigma$) (simply called as tensile strength) predictive models based on ANN and RSM. The paper also presents the effect of laser process variables on the HI and ultimate $\sigma$. The research work also emphasizes on the effect of HI on σ. The experiments were conducted based on a three-factor, three-level Box–Behnken surface statistical design. Quadratic polynomial equations were developed for proper process parametric study for its optimal performance characteristics. The experimental results under optimum conditions were compared with the simulated values obtained from the RSM and ANN model. Adequacy of the developed models was tested by analysis of variance technique. A multilayer feed-forward neural network with a Levenberg–Marquardt back-propagation algorithm was adopted to develop the relationships between the laser hardening process parameters, HI, and ultimate σ. The performance of the developed ANN models were compared with the second-order RSM mathematical models of HI and σ. There was good agreement between the experimental and simulated values of RSM and ANN. The comparison clearly indicates that the ANN models provide more accurate prediction compared to the RSM models. It has been found that there is a trend of increased tensile strength with the decrease of hardening heat input and a trend of increased tensile strength with the increase of hardening cooling rate. As heat input decreases, there will be a faster cooling rate. Considering the effect of HI on ultimate σ, it was found that the lower the heat input, the faster cooling rate. The details of experimentation, model development, testing, validation of models, effect of laser process variables on heat input and ultimate σ, effect of HI on σ, and performance comparison of RSM and ANN models are presented in the paper. The results of Box–Behnken design of RSM and ANN models also indicate that the proposed models predict the responses adequately within the limits of input parameters being used. It is suggested that regression equations can be used to find optimum conditions for HI and σ of laser-hardened commercially pure titanium material.

**Keywords** LTH · Nd: YAG laser · RSM · ANN · Heat input · Tensile strength · Box–Behnken

D. S. Badkar (✉) · K. S. Pandey
Maulana Azad National Institute of Technology,
Bhopal 462051, Madhya Pradesh, India
e-mail: dsbadkar@gmail.com

G. Buvanashekaran
Welding Research Institute, Bharat Heavy Electricals Limited,
Tiruchirappalli 620 014, Tamil Nadu, India

Published online: 06 June 2012

## 1 Introduction

Titanium and its alloys are extensively used in the aeronautical, marine, chemical, medicine, energetic, automobile, and the engineering industries, owing to their specific properties such as their light weight, high strength to weight ratio, corrosion resistance, oxidation, and excellent high temperature resistance properties (Table 1). Especially, the properties (high specific strength, modulus, corrosion resistance, etc) of titanium make it attractive for many applications.

Laser transformation hardening (LTH) is an advanced heat-treatment method to obtain hard, wear-resistant layer on surface without affecting the bulk material through the interaction of laser and material. Compared to conventional methods, it has advantages such as low thermal distortion, less post-treatment work, good controllability of laser heat source and adaptability to geometry of component, etc [1]. Laser beams, owing to their high resistance and directionality, are widely used in surface modification of many kinds of metals. Lasers have been used in a number of ways to increase the wear resistance and durability of the surface for metal [2]. Recently, automobile and machine tool industries pay attention to the technology of laser surface hardening due to a short hardening time, a small deformation after hardening, an ease of automation, and a selective hardening of part according to the function of part.

In laser surface hardening, $CO_2$ laser with multi-kW of the power has been widely used [3, 4]. In general, defocusing technology was used to harden the surface of parts as $CO_2$ laser is employed as the energy source. The defocusing technology requires a long hardening time due to utilizing of the focal area to harden the surface of parts. In addition, the hardness of the center area in the hardened area is reduced due to carburizing of the center area induced by the over melting. Because a continuous wave (CW) Nd:YAG laser has various advantages, such as a small spot size, a higher energy density, and a higher energy absorption rate of the workpiece, in comparison with the $CO_2$ laser, the research works of laser surface hardening using CW Nd:YAG laser with 1–3 kW levels of the power are actively in progress.

**Table 1** Chemical composition of commercial Titanium

| Element | % by weight |
|---|---|
| Ti | Balance |
| C | 0.10 |
| Fe | 0.20 |
| Mo | 0.003 |
| H | 0.015 |
| Zr | 0.0039 |
| O | 0.16 |
| N | 0.003 |

Response surface methodology (RSM), which is supported by software, is an empirical modelization technique derived for the evaluation of the relationship of a set of controlled experimental factors and observed results. It requires a prior knowledge of the process to achieve statistical model. Basically, this optimization process involves three major steps: estimating the coefficients in a mathematical model, predicting the response, and checking the adequacy of the model [5].

In the existing literatures, it was shown that the use of artificial neural networks (ANN) is a powerful modeling tool that has the ability to identify complex relationships from input–output data. However, no investigation to predict the effect of laser process parameters, i.e., laser power (LP), scanning speed (SS), and focused position (FP) on heat input (HI) and tensile strength (σ) of laser-hardened titanium and its alloys using ANN approach appears to have been published in the literature to date. Therefore, the present work investigates the applicability of ANN method for predicting the aforementioned parameters. The aim of this paper is to investigate the effect of laser process variables on HI and σ parameters and to evaluate the comparison of the heat input and tensile strength predictive models based on ANN and RSM by laser transformation hardening of unalloyed Titanium, nearer to ASTM Grade 3 of chemical composition using CW Nd-YAG laser beam.

## 2 Experimental design

### 2.1 Response surface methodology

Box and Behnken [7] have proposed some three-level designs for fitting response surfaces. Box–Behnken design requires an experiment number according to $N = k^2 + k + c_p$, where, $k$ is the factor number and $c_p$ is the replicate number of the central point. These designs are formed by combining two factorials with incomplete block designs. Box–Behnken is a spherical, revolving design, viewed as a cube and consists of a central point and the middle points of the edges. The resulting designs are usually very efficient in terms of the number of required runs, and they are either rotatable or nearly rotatable. A three-variable Box–Behnken design is presented by [6, 7]. It has been applied for optimization of several chemical and physical processes [8–10].

This design is generally used for fitting the second-order model. It is important to second-order model to provide good prediction throughout the region of interest. The second-order response surface design is rotatable; this means that the variance of the predicted response is the

same at all points. Rotatability is a reasonable basis for the selection of response surface design. Because the purpose of RSM is optimization at the location of optimum is unknown prior to running the experiment, it makes sense to use a design that provides equal precisions of estimation in all directions [11].

A three-factor, three-level Box–Behnken design was used for the optimization procedure. A three-factor, three-level design used is suitable for exploring quadratic response surfaces and constructing second-order polynomial models. A RSM has often been applied to optimize the formulation variables [12, 13]. The optimization procedure based on RSM includes statistical experimental designs, multiple regression analysis, and mathematical optimization algorithms for seeking the best formulation under a set of constrained equations. RSM was applied to the experimental data using statistical software; Design-expert 7.1.6. Linear and second-order polynomials were fitted to the experimental data to obtain the regression equations. The sequential $F$ test, lack-of-fit test, and other adequacy measures were used in selecting the best models. A step-wise regression method was used to fit the second-order polynomial Eq. (1) to the experimental data and to indentify the relevant model terms [14, 15].

The design consists of replicated center points and the set of points lying at the midpoint of each edge of the multidimensional cube that defines the region of interest. The nonlinear quadratic model generated by the design is of the form:

$$Y = A_0 + A_1X_1 + A_2X_2 + A_3X_3 + A_4X_1X_2 + A_5X_2X_3 + A6X_1X_3 + A_7X_1^2 + A_8X_2^2 + A_9X_3^2 + E \quad (1)$$

in which $Y$ is the measured response associated with each factor-level combination; $A_0$ is an intercept; $A_1$–$A_9$ are the regression coefficients; $X_1$, $X_2$, and $X_3$ are the factors studied; and $E$ is the error term [16]. The process variables and experimental design levels used in the design are listed in Table 2.

## 2.2 Artificial neural network

An artificial neural network is a parallel-dispensed information proceduring system. It stores the specimens with dispensed coding, thus forming a trainable nonlinear system. Neural networks closely resemble the way human brain functions. Given the inputs and longing outputs, it is also self-adaptive to the habitat so as to respond different inputs rationally. The neural network theory deals with learning from the preceding obtained data, which is named as training or learning set, and then to check the system accomplishment using test data. Computers are an integral part of day to day activities in engineering design, and engineers have utilized various applications to assist them improve their design [17–19]. ANN mimics some basic aspects of the brain functions. ANNs are based on the neural structure of the human brain, which processes information by means of interaction between many neurons; in the past few years, there has been a constant increase in interest of neural network modeling in different fields of materials science. The basic unit in the ANNs is the neuron. The neurons are connected to each other with a weight factor [20, 21]. ANNs are networks of highly interconnected neural computing elements that have the ability to respond to input stimuli and to learn to adapt to the environment. ANN includes two working phases, the phase of learning and that of recall. During the learning phase, known data sets

**Table 2** Process variables and experimental design levels used

| Variables | −1 | 0 | +1 |
|---|---|---|---|
| Laser power, LP (W) | 750 | 1,000 | 1,250 |
| Scanning speed, SS (mm/min) | 1,000 | 2,000 | 3,000 |
| Focused position, FP (mm) | −30 | −20 | −10 |

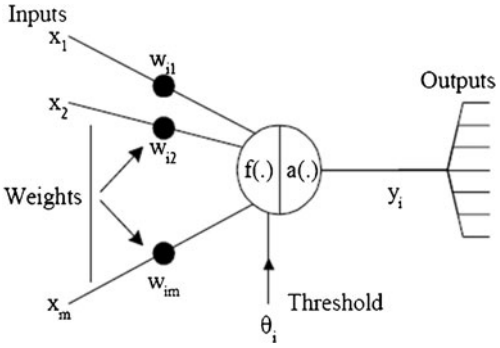


**Fig. 1** The mathematical model of neuron [24]

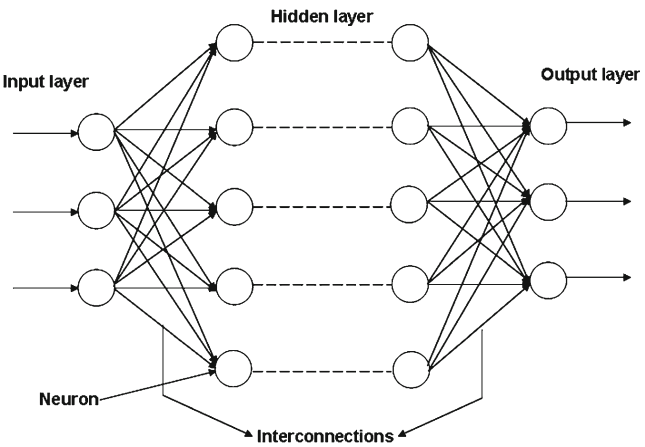


**Fig. 2** The architecture of a feed-forward type multilayer neural network

**Table 3** Design matrix with code independent process variables

| Exp. no | Run order | Laser power (LP); W | Scanning speed (SS); mm/min | Focused position (FP); mm |
|---|---|---|---|---|
| 1 | 14 | −1 | −1 | 0 |
| 2 | 1 | 1 | −1 | 0 |
| 3 | 4 | −1 | 1 | 0 |
| 4 | 8 | 1 | 1 | 0 |
| 5 | 3 | −1 | 0 | −1 |
| 6 | 5 | 1 | 0 | −1 |
| 7 | 6 | −1 | 0 | 1 |
| 8 | 16 | 1 | 0 | 1 |
| 9 | 10 | 0 | −1 | −1 |
| 10 | 13 | 0 | 1 | −1 |
| 11 | 7 | 0 | −1 | 1 |
| 12 | 15 | 0 | 1 | 1 |
| 13 | 12 | 0 | 0 | 0 |
| 14 | 11 | 0 | 0 | 0 |
| 15 | 9 | 0 | 0 | 0 |
| 16 | 17 | 0 | 0 | 0 |
| 17 | 2 | 0 | 0 | 0 |

are commonly used as a training signal in input and output layers. The recall phase is performed by one pass using the weight obtained in the learning phase. ANN is now a well established tool, and details about it can be found elsewhere. Various nomenclatures are used to describe neural network paradigms [22, 23]. Whereas a single-layer network has single input/output units, a multilayer network has one or more hidden units between input and output layers (Fig. 1).

A back-propagation (BP) neural network is a multilayer neural network which uses gradient-descent technique analogous to error minimization. A neural network is characterized by the pattern of connections between the neurons; this is called the network architecture. Various nomenclatures are used to describe neural network paradigms [20–22]. Whereas a single-layer network has single input/output units, a multilayer network has one or more hidden units between input and output layers (Fig. 1). The information included in the illustration data was acquired via the improved BP learning algorithm. The parameters of the BP network were defined as follows:

The input vectors $X = [x_0, x_1, \ldots, x_n]^T$
The output vectors $[Y = y_0, y_1, \ldots, y_{m1}]^T$

where, the symbols $n$, $h$, and $m$ represented the number of neurons in the input layer, the hidden layer, and the output layer, sequentially [25].

### 2.3 Experimental data set interpolation using ANN

As previous research has amply shown, neural networks are effective tools when it comes to modeling unknown or semi-unknown processes [26]. In this case, ANN was used in order to interpolate the incomplete experimental data set that was available for the analysis. The experimental data coming from the experimental trials are amended in order to be suitable for statistical analysis.

As different network formats are proposed in the literature, the first problem to be solved is what type of network should be adopted. The results of previous analyses showed that the neural network used was the multilayer feed-forward type (MFNN) in 95 % of the cases [27]. The frequent use of this type of network is mainly due to the fact that it acts as a universal interpolator in a wide range of cases in which input variables are to be related to a set of output variables. These networks are of the supervised learning type, in that the input/output relation can only be learned based on a set of training data (Fig. 2). The typical architecture of an MFNN is shown in Fig. 2. It includes an input layer ($x$), one or more hidden layers, and an output layer. Each layer consists of one or more neurons linked

**Table 4** Experimental measured responses

| Exp. no | Run order | Heat input (HI); J/cm | Ultimate Tensile strength(σ); MPa | Exp. no | Run order | Heat input (HI); J/cm | Ultimate tensile strength (σ); MPa |
|---|---|---|---|---|---|---|---|
| 1 | 14 | 450 | 438 | 10 | 13 | 200 | 457 |
| 2 | 1 | 750 | 430 | 11 | 7 | 600 | 430 |
| 3 | 4 | 150 | 460 | 12 | 15 | 200 | 455 |
| 4 | 8 | 250 | 452 | 13 | 12 | 300 | 450 |
| 5 | 3 | 225 | 454 | 14 | 11 | 300 | 449 |
| 6 | 5 | 375 | 445 | 15 | 9 | 300 | 447 |
| 7 | 6 | 225 | 449 | 16 | 17 | 300 | 451 |
| 8 | 16 | 375 | 443 | 17 | 2 | 300 | 448 |
| 9 | 10 | 600 | 432 | | | | |

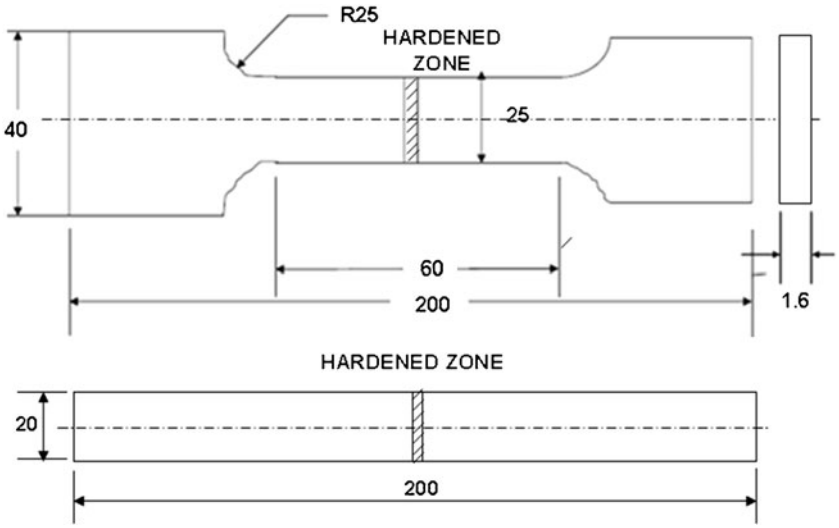


**Fig. 3** Schematic sketch of tensile test specimen, as per AWS B4.0

together by weights used to convey data from all the neurons of the previous layer to all those present in the subsequent layer.

A commercial Microsoft Windows-based ANN software, Matlab Version R2007b (The Math Works, Natick, MA) was used throughout the study. This software allows the user to select the number of hidden layers and hidden layer nodes (neurons), iterations used during the model training, learning algorithm, and transfer functions. After training the network successfully, it has been tested by using the known test data. Statistical methods were used to compare the results produced by the network. Errors occurring at the learning and testing stages are called the root mean square (RMS), absolute fraction of variance or correlation coefficient ($R^2$), and mean absolute error percentage values. These are defined as follows, respectively:

$$RMS = \left[\left(\frac{1}{P}\right)\sum |t_j - o_j|^2\right]^2$$

$$R^2 = \left[\frac{\sum_{\mathrm{j}} (t_{\mathrm{j}} - o_{\mathrm{j}})}{\sum_{\mathrm{j}} (o_{\mathrm{j}})^2}\right]$$

$$\text{Mean absolute error percentage} = \left(\frac{1}{P}\right)\left[\sum_{\mathrm{j}} \frac{t_{\mathrm{j}} - o_{\mathrm{j}}}{t_{\mathrm{j}}} \times 100\right]$$

**Table 5** ANOVA table for heat input reduced quadratic model

| Source | Sum of squares | df | Mean square | *F value* | *p* value Prob > *F* | |
|---|---|---|---|---|---|---|
| Model | 433,602.9412 | 4 | 108,400.74 | 1040.647 | <0.0001 | Significant |
| LP | 61,250.0000 | 1 | 61,250 | 588 | <0.0001 | |
| SS | 320,000.0000 | 1 | 320,000 | 3,072 | <0.0001 | |
| LP × SS | 10,000.0000 | 1 | 10,000 | 96 | <0.0001 | |
| $SS^2$ | 42,352.9412 | 1 | 42,352.941 | 406.5882 | <0.0001 | |
| Residual | 1,250.0000 | 12 | 104.16667 | | | |
| Lack-of-fit | 1,250.0000 | 8 | 156.25 | | | |
| Pure error | 0.0000 | 4 | 0 | | | |
| Corrected total | 434,852.9412 | 16 | | | | |
| Std. Dev. | 10.2062 | | | | | |
| Mean | 347.059 | | | | | |
| C.V. % | 2.94077 | | | | | |
| PRESS | 5515.52 | | | | | |
| *R*-Squared | 0.9971 | | | | | |
| Adj *R*-Squared | 0.9962 | | | | | |
| Pred *R*-Squared | 0.9873 | | | | | |
| Adeq Precision | 103.883 | | | | | |

**Table 6** ANOVA table for ultimate tensile strength reduced quadratic Model

| Source | Sum of squares | df | Mean square | *F value* | *p* value Prob > *F* | |
|---|---|---|---|---|---|---|
| Model | 1322.1695 | 5 | 264.4339 | 161.01 | < 0.0001 | Significant |
| LP | 120.125 | 1 | 120.125 | 73.1424 | < 0.0001 | |
| SS | 1104.5 | 1 | 1104.5 | 672.5142 | < 0.0001 | |
| FP | 15.125 | 1 | 15.125 | 9.2094 | 0.0114 | |
| SS^2 | 71.6148 | 1 | 71.6148 | 43.6052 | < 0.0001 | |
| FP^2 | 7.9064 | 1 | 7.9064 | 4.8141 | 0.0506 | |
| Residual | 18.0658 | 11 | 1.6423 | | | |
| Lack-of-Fit | 8.0658 | 7 | 1.1522 | 0.4609 | 0.8253 | Not significant |
| Pure Error | 10 | 4 | 2.5 | | | |
| Corrected Total | 1340.2353 | 16 | | | | |
| Std. Dev. | 1.2815 | | | | | |
| Mean | 347.059 | | | | | |
| C.V. % | 0.2870 | | | | | |
| PRESS | 39.274 | | | | | |
| *R*-Squared | 0.9865 | | | | | |
| Adj *R*-Squared | 0.9804 | | | | | |
| Pred *R*-Squared | 0.9707 | | | | | |
| Adeq Precision | 41.046 | | | | | |

where $P$ is the number of patterns, $t_j$ is the target value, $o_j$ is the output value.

A multilayer feed-forward back-propagation network, which was created by generalizing the Levelberg–Marquardt's learning rule to multiple layer networks and nonlinear differential transfer functions, was used for training of experimental results and to predict the laser-hardened parameters HI and σ. Our network architecture consisted of an input layer with three neurons, an output layer with two neurons, and a hidden layer with four neurons (Fig. 4). The number of hidden nodes in a network is critical to network performance. Too few nodes can lead to underfitting. Too many nodes can lead the system toward memorizing the patterns in the data [28]. Therefore, hidden layer with four neurons selected and resulted with uniformly distributed predicted values of outputs nearer to experimental values with coefficient determination *R*-squared almost equal 1.

Input vectors and the output vectors (response) were used to train the network until it could approximate a function (i.e., associate input vectors with specific output vectors). Trained back-propagation networks tend to give reasonable answers when presented with inputs that they have never seen.

**Table 7** Training parameters used

| | |
|---|---|
| The number of layers | 3 |
| The number of neurons on the layers | Input: 3, Hidden: 4 , Output: 2 |
| Activation functions for hidden and output layers | Tan-sigmoid, purelin |
| Training parameters Learning rule | Back-propagation, Levenberg–Marquardt's learning rule |
| Number of iteration or epoches | 181 |
| Momentum constant | 0.95 |
| Acceptable mean-squared error (MSE) goal | 0 |
| Number of training sets used | 1 |

## 3 Experimental methodology

The experiments are conducted on a given unalloyed Titanium alloy substrate with chemical composition given in Table 1. The chemistry is nearer to ASTM Grade 3. The thickness of the substrate selected is 1.6 mm to simulate the majority of the industrial applications that is in practice at present. For conducting the experiments on the substrate, the materials surface is cleaned properly with suitable agents.

A 2-kW, CW mode Nd:YAG laser beam device from GSI Lumonics is used as machining tool in this study as shown in Fig. 1. Unlike the 10.6-μm wavelength of the $CO_2$ laser beam, the wavelength of the Nd:YAG laser beam is only 1.064 μm. The low-beam energy prevents the surface of the hardening area from overheating and ensures that the heat affected zone is small.

The experiment was carried out according to the Box–Behnken design matrix in a random order to avoid any systematic error. A spherical beam configuration is used throughout the study. The laser beam is transported through

a fiber optic cable to the work center. Siemens 802 CNC controller is providing the process control during the experiments. The work center is having *x*, *y*, and rotational movement for processing applications. The laser source, work center, and the controls are interfaced. Cooling is ensured by a chiller and a cooling tower. For the study, a 120-mm focal optic is employed with varying beam spot size depending on defocus distance to obtain a wider scan area. Argon gas is employed as shielding medium with a constant flow rate of 8 lpm throughout the experimental work. Transverse sectioned specimens were cut from laser-hardened bead-on trial of unalloyed Titanium sheet having 1.6 mm thickness and mounted. Standard metallographic was made for each transverse sectioned specimens.

For the microstructure observation, the transverse section cut laser-hardened specimens were ground with SiC paper to # 1,500, and then polished by 1-μm $Al_2O_3$ powder. The microstructure of the hardened surface observed using an optical microscope (with image processing computer-controlled software) with digital micrometers attached to it with an accuracy of 0.001 mm, which allow to measure in x-axes and y-axes after the polished surface was acid etched by a solution of Kroll's reagent: 10 ml of HF, 5 ml $HNO_3$, 85 ml water; procedure: swab 3–20 s.

The measured laser-hardened bead profile parameters "responses" were recorded. The design matrix and the measured responses are shown in Tables 3 and 4.

The schematic diagram of specimens which are used for tensile test and their dimensions are given in Fig. 3. All the specimens were obtained in the same orientation from the laser-hardened plate. The single-pass laser beam transformation hardening experiments were conducted on a given commercially pure Ti or unalloyed titanium substrate. The thickness of the substrate selected is 1.6 mm to stimulate the majority of industrial applications that is in practice at present. Pre-welding cleaning procedures and steps to protect the molten weld zone were carried out to avoid the contamination of the weld. The test piece (100×100× 1.6 mm) is pickled in a solution of $HNO_3$, HF, and $H_2O$ (27 vol. % $HNO_3$, 3 vol. % HF, and balance $H_2O$) and the surface is properly cleaned with acetone before laser welding trials.

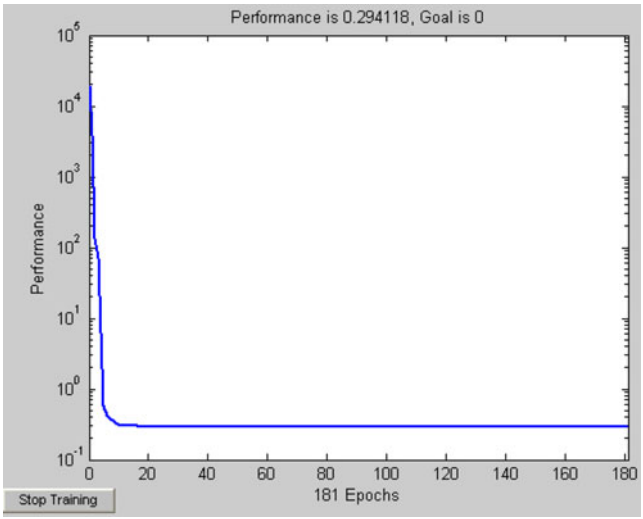


**Fig. 5** Training performance of neural network for design data

## 4 Results and discussions

In the laser transformation hardening process of unalloyed titanium, the LP ranged from 750 to 1,250 W, SS ranges 1,000–3,000 mm/min, and FP ranges between −10 and −30 mm, respectively. The results of the laser-hardened-bead profile were measured according to the design matrix with coded independent process variables in Table 3 using the transverse sectioned specimens and the optical microscope mentioned earlier; the measured responses are listed in Table 4. Analyzing the measured responses by the Design-expert software, the fit summary output indicates that the linear model is statistically significant for hardened bead width "the second response" therefore it will be used for further analysis.

### 4.1 Analysis of variance

The adequacy of the developed models were tested using the analysis of variance (ANOVA) technique and the results of the linear and quadratic order response surface model fitting in the form of ANOVA are given in Tables 5 and 6. The test for significance of the regression models, the test for

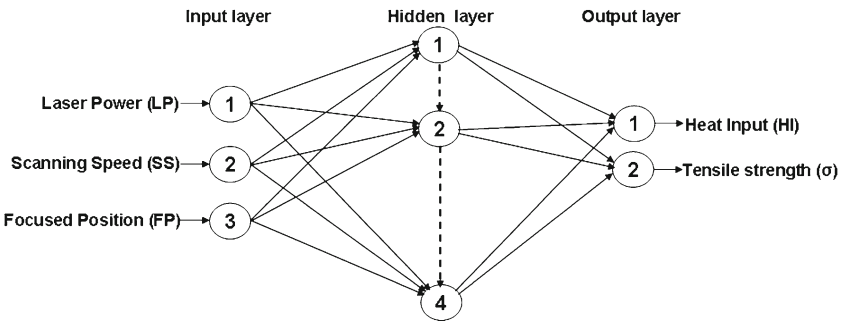


**Fig. 4** Schematic diagram showing the multiple layer structure of neural network for design data and their interconnectivity between the nodes of the network

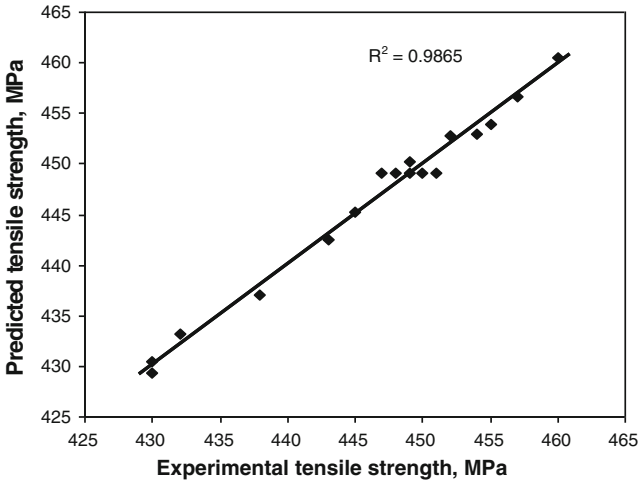


**Fig. 6** Scatter diagram of heat input for RSM model (design data)

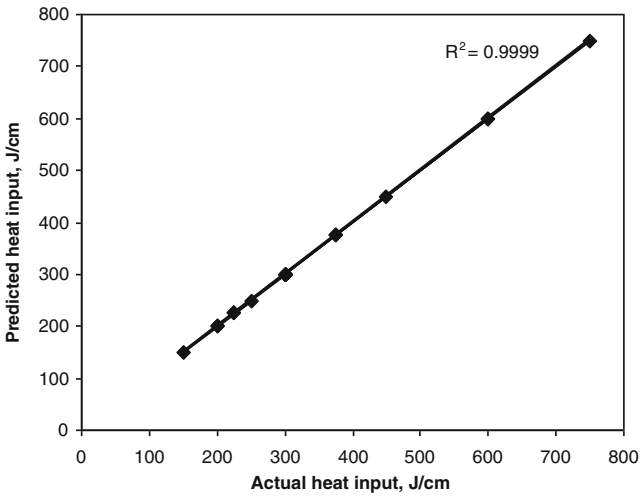


**Fig. 8** Scatter diagram of heat input for ANN model (design data)

significance on individual model coefficients, and the lack-of-fit test were performed using the same statistical Design-expert 7 software package. By selecting the step-wise regression method, which eliminates the insignificant model terms automatically, the resulting ANOVA (Tables 5 and 6) for the response surface quadratic models summarize the analysis of variance of each response and show the significant model terms. The same tables show also the other adequacy measures $R^2$, adjusted $R^2$, and predicted $R^2$. The coefficient of determination $R^2$ indicates the goodness of fit for the model. In this case, all the values of coefficient of determination $R^2$ are nearly equal to 1. Clearly, we must have $0 \leq R^2 \leq 1$, with larger values being more desirable. The adjusted coefficient of determination $R^2$ or "adjusted" $R^2$ is a variation of the ordinary $R^2$ statistic that reflects the number of factors in the model. The entire adequacy measures are closer to 1, which is in reasonable agreement and indicate adequate models. The adequate precision "Adeq Precision" compares the range of the predicted value at the design points to the average prediction error. Adequate precision measures signal to nose ratio. A ratio greater than 4 is desirable. In all cases, the values of adequate precision are dramatically greater than 4. The adequate precision ratio above 4 indicates adequate model discrimination. The ANOVA (Tables 5 and 6) also shows the model terms standard Std. Dev, Mean, C.V, and PRESS. "Std. Dev." Standard deviation is a square root of the error mean square, $\sqrt{MS_E}/\bar{y}$, and "C.V." is the coefficient of variation, defined as $(\sqrt{MS_E}/\bar{y})$ 100, where $\bar{y}$ = Mean. The coefficient of variation, "C.V.", measures the unexplained or residual variability in the data as a percentage of the mean of the response variable. At the same time, a relatively lower

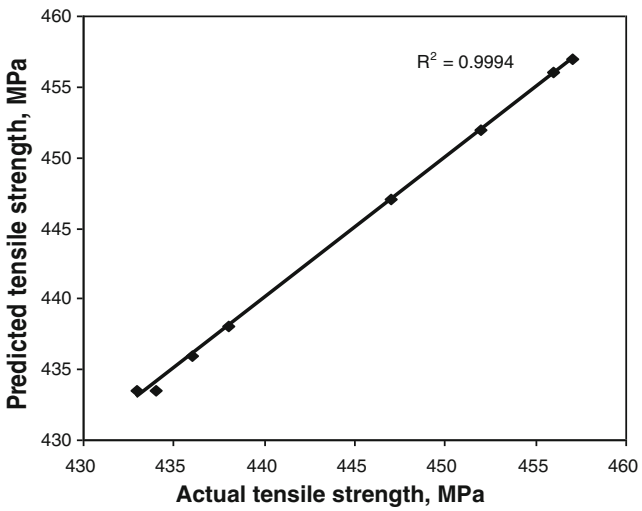


**Fig. 7** Scatter diagram of for tensile strength RSM model (design data)

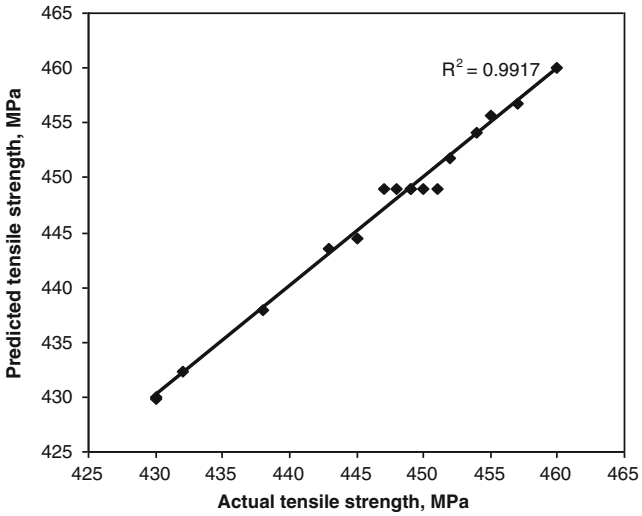


**Fig. 9** Scatter diagram of for tensile strength ANN model (design data)

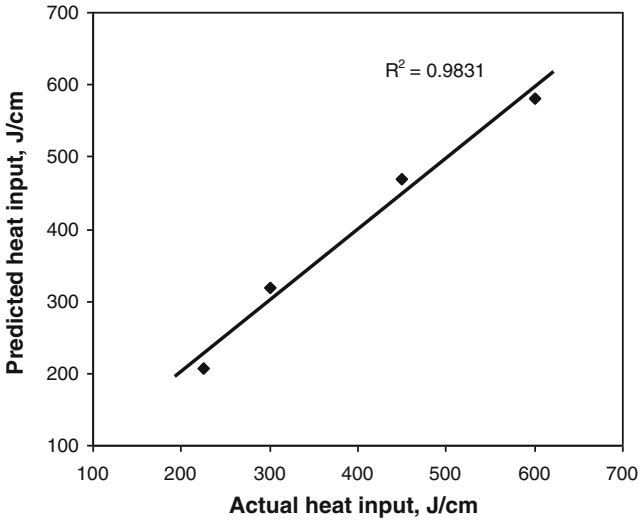


**Fig. 10** Scatter diagram of heat input for RSM model (validation data)

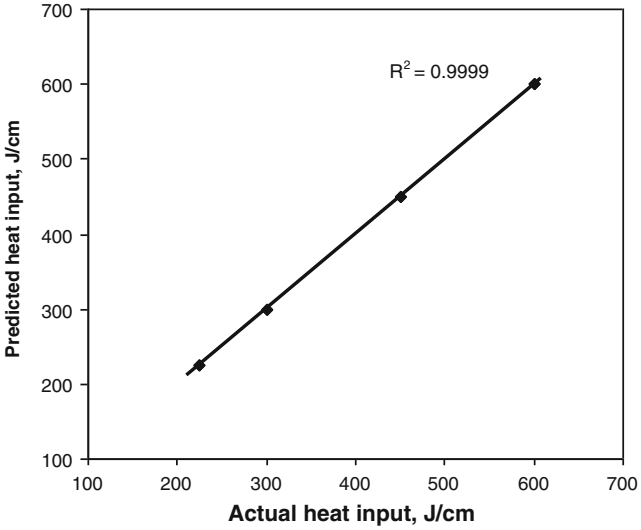


**Fig. 12** Scatter diagram of heat input for ANN model (validation data)

values of the coefficient of variation, C.V., from the Tables 5 and 6 indicate improved precision and reliability of the conducted experiments. "PRESS" stands for "Prediction error sum of squares," and it is a measure of how well the model for the experiment is likely to predict the responses in a new experiment. Small values of PRESS are desirable. In all the cases, the values of PRESS are considerably small.

The values of "Probability > *F*" in Tables 5 and 6 for all models are less than 0.0500, which indicate that all models are significant. In all cases, the "lack-of-fit" values imply that it is not significant relative to the pure error. Non-significant lack-of-fit is desired and it is good.

## 4.2 RSM modeling

A step-wise multiple regression method was used to fit the second-order polynomial equation to the experimental data and to identify the relevant model terms HI and σ using the same design expert software. By selecting the step-wise regression method, which eliminates the insignificant model terms automatically, the resulting ANOVA for the reduced models summarize the analysis of variance of each response and show the significant model terms. The following mathematical models in terms of coded and actual factors were obtained for the HI and σ, respectively. The final mathematical models in terms of

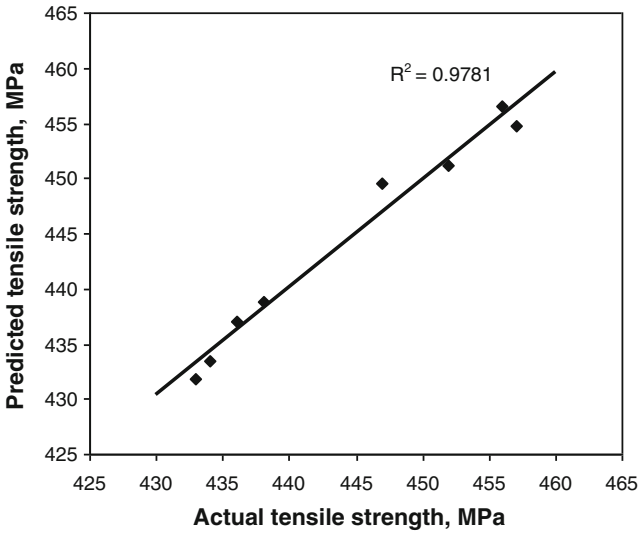


**Fig. 11** Scatter diagram of for tensile strength RSM model (validation data)

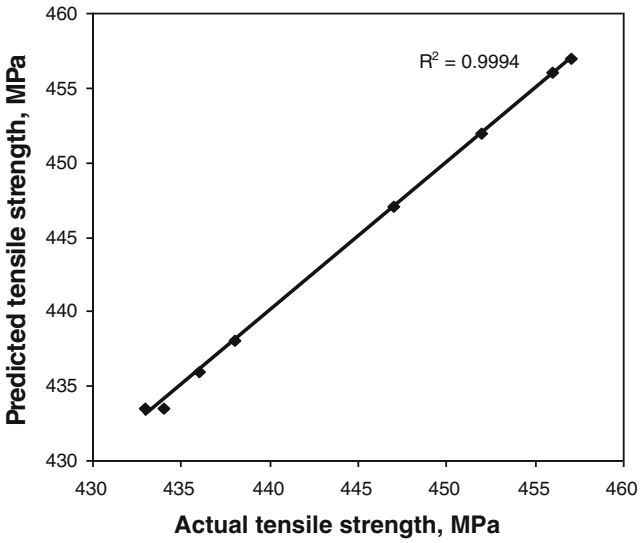


**Fig. 13** Scatter diagram of for tensile strength ANN model (validation data)

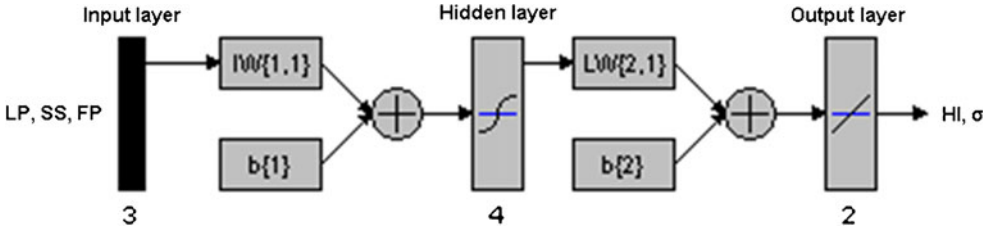


**Fig. 14** Schematic diagram showing the trained neural network architecture for the validation data

coded factors as determined by design expert software are shown below:

$$HI = +300.00 + 87.50 \times LP - 200.00 \times SS - 50.00 \times LP \times SS + 100.00 \times SS^2 \quad (2)$$

$$\sigma = +449.05 - 3.88 \times LP + 11.75 \times SS - 1.38 \times FP - 4.12 \times SS^2 - 1.37 \times FP^2 \quad (3)$$

While the following final empirical models in terms of actual factors:

$$HI = +350.00 + 0.75 \times LP - 0.40 \times SS - 2.0E - 004 \times LP \times SS + 1.0E - 004 \times SS^2 \quad (4)$$

$$\sigma = +416.355 - 0.0155 \times LP + 0.0282 \times SS - 0.6849 \times FP - 4.118E - 006 \times SS^2 - 0.01368 \times FP^2 \quad (5)$$

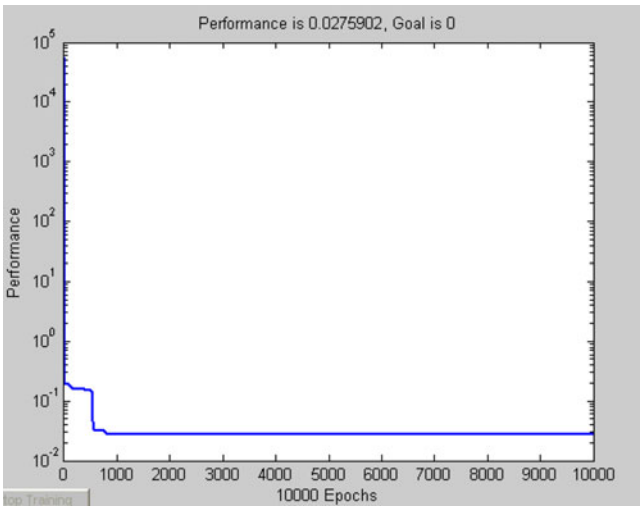


**Fig. 15** Training performance of neural network for validation data

## 4.3 Modeling with neural networks

Laser transformation hardened test specimens heat input and tensile strengths were modeled using MATLAB program. A commercial Microsoft Windows-based ANN software, Matlab Version 7.5.0.0.342 (R2007 b) (The Math Works Inc.) was used throughout the study. This software allows the user to select the number of hidden layers and hidden layer nodes (neurons), iterations used during the model training, learning algorithm, and transfer functions. In the experiment, based on the three-factor, three-level Box–Behnken design was used for the optimization procedure. All 17 batches were prepared, and laser -hardened parameters HI and σ of these batches were all used for training. Learning rate and error goal were selected on a trial and error basis in such a way so as to keep the minimum distance between the actual and predicted values.

Laser process parameters/variables such as LP, SS, and FP were employed as inputs, and HI and σ were recorded as output parameters. Training parameters used in this investigation were presented in Table 7.

In the present study, the neural network architecture consists of an input layer with three neurons, an output layer with two neurons, and a hidden layer with four neurons as shown in Fig. 4. One of the most vital tasks in constructing the ANNs is the choice of the number of hidden layers and the number of neurons. In this study, a number of tests are performed by varying the number of hidden layers and the number of neurons in the hidden layer. The architecture with one hidden layer with four neurons is found to be good for the best accuracy with normally distributed ANN outputs with experimental values. The "tansig" tangent sigmoidal transfer function is used in the hidden layer and "purelin" linear activation function is used at the output layer. In order to calculate the HI and σ mathematical formulations can be derived from the resulting weights and the activation functions used in the ANN. Seven networks are trained and validated to obtain the reliable results by varying the number of neurons and hidden layers. Of the seven networks selected for training (1HX4N, 1HX5N, 1HX6N, 3HX7N, 1HX8N, 1HX9N, and 1HX10N), the network with one hidden layer with four neurons gave the best coefficient of multiple determinations. The optimum architecture is taken as 3-4-2 (three neurons in the output layer, four neurons in the hidden layer, and two neurons in output layer) by trial,

**Table 8** Confirmation of experiments

| Exp. no | Run order | LP | SS | FP | Experimental values | | RSM values | | ANN values | |
|---|---|---|---|---|---|---|---|---|---|---|
| | | | | | HI | TS (σ) | HI | TS (σ) | HI | TS (σ) |
| 1 | 5 | 750 | 1,000 | −20 | 450 | 438 | 468.75 | 438.75 | 449.9958 | 438.0284 |
| 2 | 8 | 1,000 | 1,000 | −20 | 600 | 434 | 581.25 | 433.50 | 599.9941 | 433.5389 |
| 3 | 3 | 750 | 2,000 | −20 | 225 | 456 | 206.25 | 456.50 | 225.0015 | 456.0432 |
| 4 | 6 | 1,000 | 2,000 | −20 | 300 | 452 | 318.75 | 431.75 | 299.9999 | 451.9902 |
| 5 | 1 | 750 | 1,000 | −10 | 450 | 436 | 468.75 | 437.00 | 450.0030 | 435.9519 |
| 6 | 4 | 1,000 | 1,000 | −10 | 600 | 433 | 581.25 | 431.75 | 600.0067 | 433.4700 |
| 7 | 2 | 750 | 2,000 | −10 | 225 | 457 | 206.25 | 454.75 | 224.9994 | 456.9531 |
| 8 | 7 | 1,000 | 2,000 | −10 | 300 | 447 | 318.75 | 449.50 | 299.9996 | 447.0243 |

when the mean square error (MSE) decreased gradually and become stable, and the training and testing error produced satisfactory results. In all the cases, the MSE obtained was same value with 0.294118. Therefore, hidden layer with less number of neurons with four was selected and resulted with uniformly distributed predicted values of outputs nearer to experimental values with coefficient determination *R*-squared almost equal 1. Input vectors and the output vectors (response) were used to train the network until it could approximate a function (i.e., associate input vectors with specific output vectors). Figure 5 shows the training performance curve of neural network. The coefficient of determination *R*-squared indicates the goodness of fit for the model. In this case, the value of the determination coefficient for HI and σ response surface models are 0.9999 and 0.9917, respectively. *R*-squared values for all the models are nearly equal to 1, which indicates the significance of the model.

The tolerance limit for the MSE is set to 0. The MSE of the training set become stable at 0.294118 when the number of iteration reaches to 181 epoches .The closeness of the training and testing errors validates the accuracy of the model. Thus, good, sufficient, higher values of coefficient of determination (*R*-squared) with tendency of reaching 1 and low values of error are obtained in testing the developed models for the prediction of HI and σ outputs using neural networks.

### 4.4 Validation of the models

Figures 6, 7, 8, 9, 10, 11, 12 and 13 show the relationship between the actual and predicted values of the HI and σ for design and validation data of RSM and ANN models, respectively. Since the residuals tend to be close to the diagonal line, these figures indicate that the developed models for design and validation data are adequate, because the residuals in prediction of each response are minimal. This means that actual/experimental values are very close to the predicted values of RSM and ANN models for both design and validation data (meaning that error between actual and predicted values are very small). Furthermore, to verify the adequacy of the developed models, eight confirmation experiments of $2^3$ full factorial design with three factors with two levels were carried out using new test conditions but are within the experimental range defined early. The trained neural network architecture for the validation data obtained also consists of the identical training parameters of design data with an input layer with three neurons, an output layer with two neurons, and a hidden layer with four neurons as shown in Fig. 14. Figure 15 shows the training performance curve of neural network. In this case, the values of the determination coefficients for HI and σ are 0.9831, 0.9781 for RSM model and 0.9999, 0.9994 for ANN model, respectively. *R*-squared values for all the models are nearly

**Table 9** Comparison of predictive capacity of RSM and ANN for the design and validation data

| Parameters | Design data | | | | Validation data | | | |
|---|---|---|---|---|---|---|---|---|
| | Heat input | | Tensile strength | | Heat input | | Tensile strength | |
| | RSM | ANN | RSM | ANN | RSM | ANN | RSM | ANN |
| $R^2$ | 0.9971 | 0.9999 | 0.9865 | 0.9917 | 0.9831 | 0.9999 | 0.9781 | 0.9994 |
| Mean absolute % error | 2.0917 | 0.0117 | 0.1970 | 0.1147 | 5.4700 | 5.95E-04 | 0.2675 | 0.0338 |
| RMSE | 8.5749 | 0.0438 | 1.0309 | 0.8099 | 18.750 | 0.00367 | 1.3919 | 0.2349 |

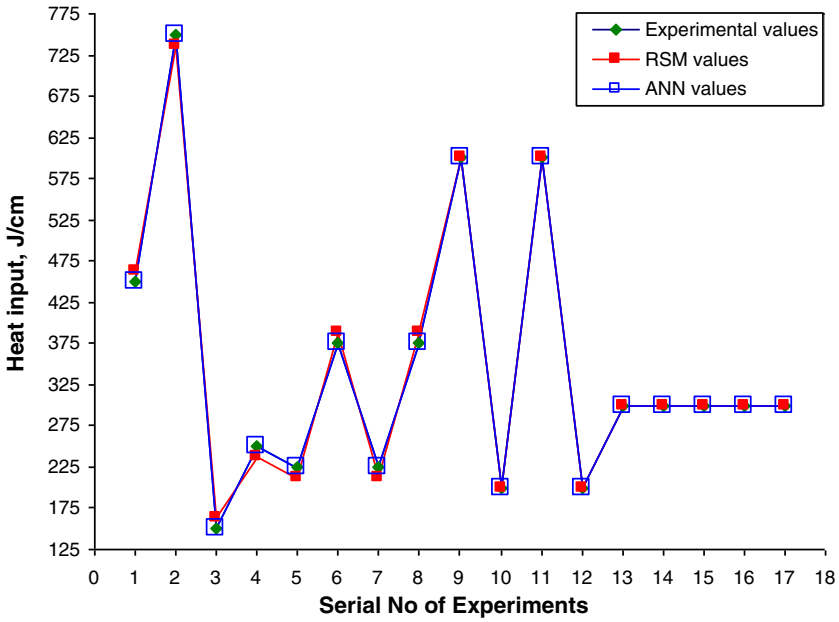


**Fig. 16** Comparison between experimental, RSM, and ANN values of heat input

equal to 1, which indicates the significance of the model. From the figures and results, it has been also observed that the values of correlation coefficients for both design and validation data of their respective RSM and ANN models are nearly analogous to each other and all are nearly equal to 1.

The tolerance limit for the MSE is set to 0. The MSE of the training set become stable at 0.0275902 when the number of iteration reaches to 10,000 epochs. The closeness of the training and testing errors validates the accuracy of the model. Table 8 summarizes the experimental condition of the validation data with the actual experimental and predicted values of RSM and ANN models.

### 4.5 Comparison between ANN and RSM models

The prediction performance of RSM and ANN models in terms of coefficient of determination (correlation coefficient or *R*-squared), mean absolute error %, and root mean square error (RMSE) are shown in Table 9. It shows that in all the cases, the ANN models had better prediction than RSM models. The RSM and ANN laser-hardened models of HI and σ so developed were compared on the basis of their coefficient of determination(*R*-squared), prediction accuracy, and ability to provide the direct and interaction effects of process parameters.

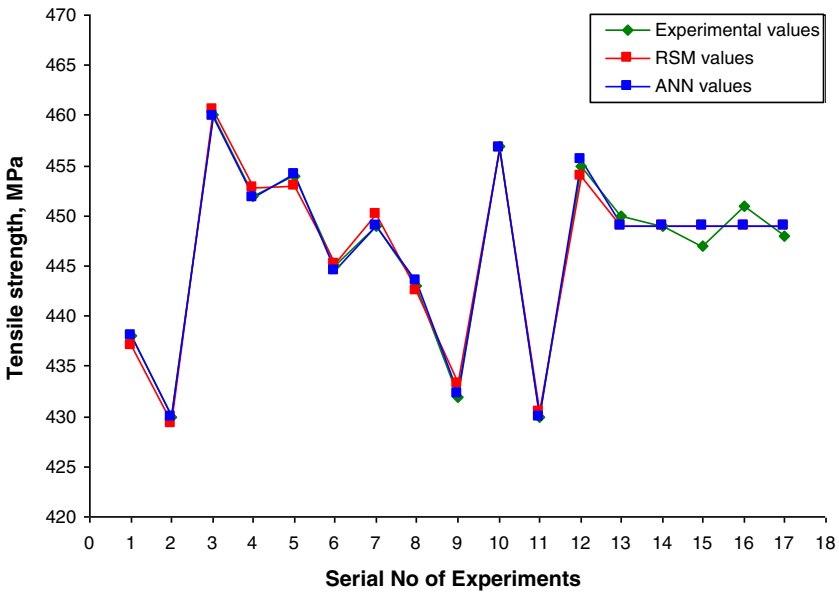


**Fig. 17** Comparison between experimental, RSM, and ANN values of tensile strength

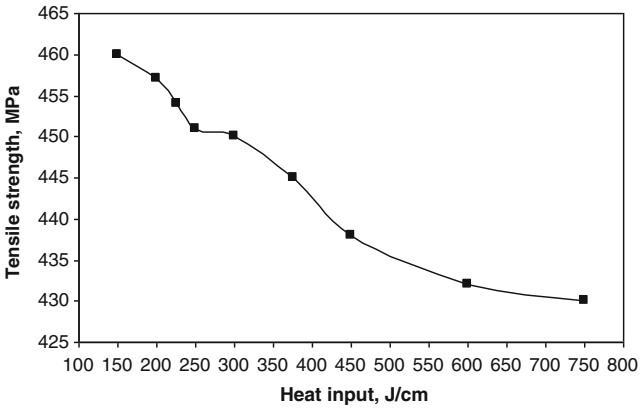


**Fig. 18** The relationship between tensile strength and heat input

### *4.5.1 Coefficient of determination (R-squared)*

Figures 6, 7, 8, 9, 10, 11, 12 and 13 shows the relationship between the actual and predicted values of HI and σ for RSM and ANN models, respectively. A comparison of the correlation between the experimental and the predicted values of RSM and ANN models for testing the design and validation data patterns are represented in the form of scatter diagrams, as illustrated in Figs. 6, 7, 8, 9, 10, 11, 12 and 13 of HI and σ, respectively. These figures indicate that the developed models for RSM and ANN models are adequate because the residuals in prediction of each response are minimal, since the residuals tend to be close to the diagonal line. This means that the actual values of heat input and tensile strength are very close to the corresponding predicted values of heat input and tensile strength for RSM and ANN models for both design and validation data (meaning that error between actual and predicted values are very small).The coefficient determination or correlation coefficient (*R*-squared) between the predicted and actual or experimental values is a measure of how well the variation in the predicted is explained by the actual values. An *R*-squared value of 1 indicates perfect correlation between actual and predicted values. In the present case, the *R*-squared values of ANN-based models of HI and σ are more than the RSM-based models of HI and σ for both design and validation data, which clearly indicates that the prediction accuracy of the ANN model is higher as compared to the RSM model. From these figures and Table 9, it is observed that *R*-squared values for ANN models 0.9999, 0.9917 are higher than those obtained for RSM models 0.9971, 0.9865 for of HI and σ models respectively. In case of validation data, *R*-squared values for ANN models 0.9999, 0.9994 are also higher than the RSM models 0.9831, 0.9781 for of HI and σ models, respectively. For all the models, the coefficient of determination is almost equal to 1. This confirms the goodness of fit for RSM and ANN models. In all the cases of design data as well as for validation data, ANN models ensured better *R*-squared values as compared to RSM models.

### *4.5.2 Prediction accuracy*

The RSM and ANN models were tested with all 17 design data sets of full factorial Box–Behnken design of experiments used for the model development. The RSM and ANN models were also tested for $2^3$ full factorial design for validation data for confirmation of experiments. For each input combination, the predicted values of HI and σ output

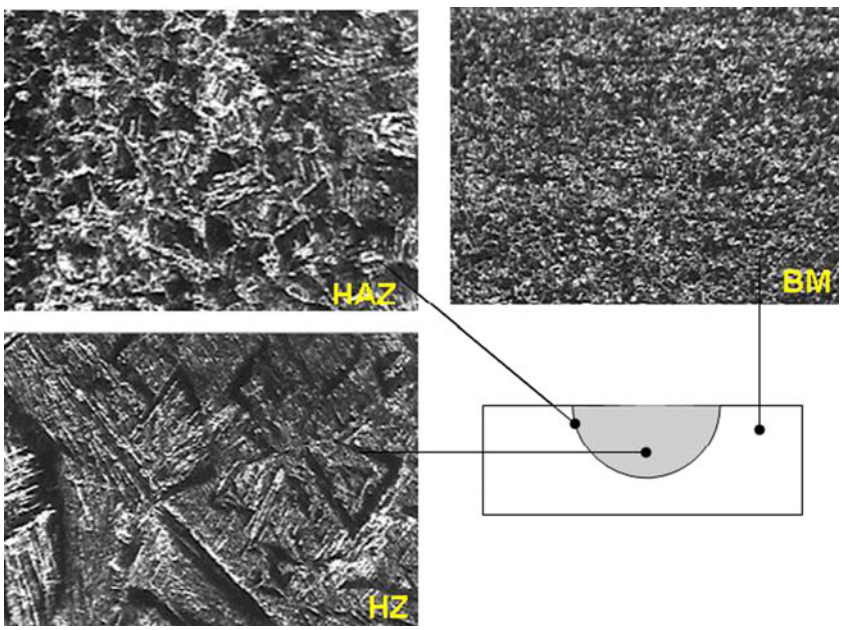


**Fig. 19** Microstructure of the commercially pure Titanium (specimen B) laser hardened at 750 W (LP), 3,000 mm/min (SS), and focused position (FP=−20 mm) with lower value of heat input 150 J/cm at ×200

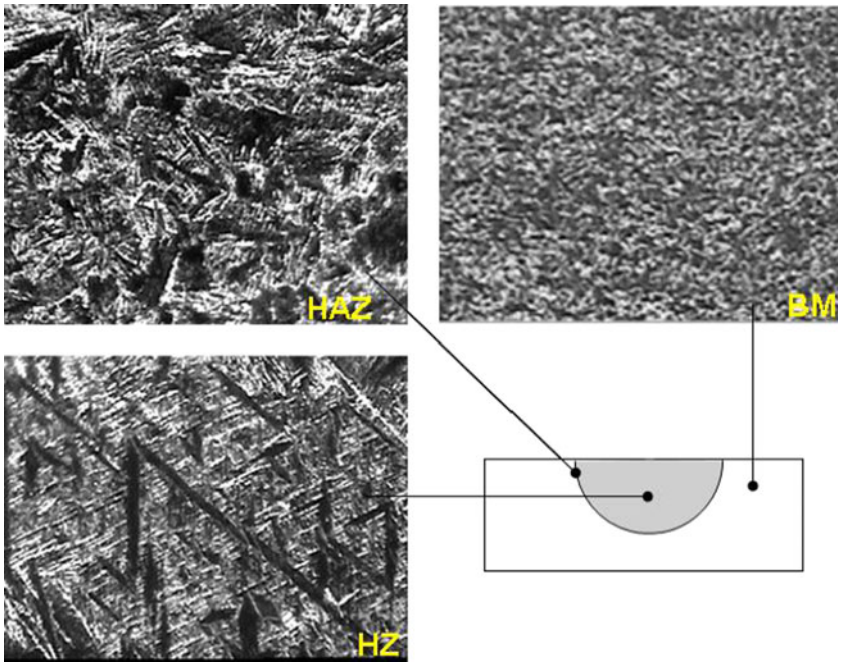


**Fig. 20** Microstructure of the commercially pure Titanium (specimen A) laser hardened at 1, 250 W (LP), 1,000 mm/min (SS), and focused position (FP=−20 mm) with higher value of heat input 750 J/cm at ×200

responses were compared with the respective experimental values and the absolute or mean percentage error is computed using the following equation:

$$\text{Mean absolute error } \% = \frac{1}{p}\left|\frac{y_{i,\exp t} - y_{i,\text{pred}}}{y_{i,\exp t}}\right|$$

Where $p$ is the number of patterns, $y_{i,\exp t}$ is the experimental value, and $y_{i,\text{pred}}$ is the predicted value of the response for the $i$th trial by the RSM and ANN models. Table 9 shows the comparison of RSM and ANN models in terms of three criterion of validity, coefficient of determination, mean absolute error %, and RMSE for both design and validation data.. Therefore, considering the results, it is confirmed that ANN model predicts more accurately than the RSM model.

The mean absolute percentage error in the ANN model prediction of HI and σ are 0.0117 and 0.1147 %, respectively, while for the RSM model prediction, those were found to be around 2.0917 and 0.1970 %, respectively. Similarly, in case of validation data, the mean absolute percentage error in the ANN model prediction of HI and σ are 5.95E-04 and 0.0338 %, respectively, while in the RSM model prediction, these were found to be around 5.4700 and 0.2675 %, respectively. For both the output parameters of

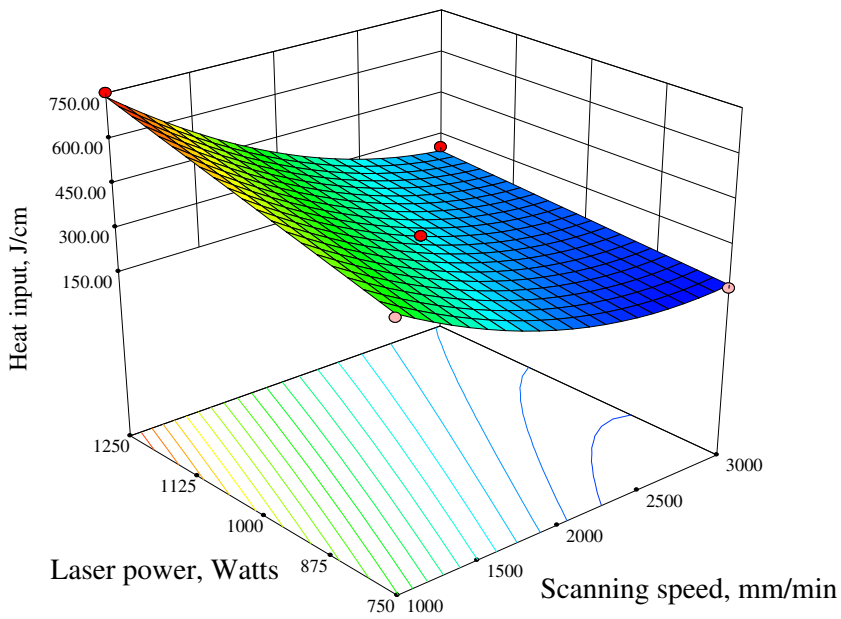


**Fig. 21** 3D graph shows the effect of LP and SS on the heat input

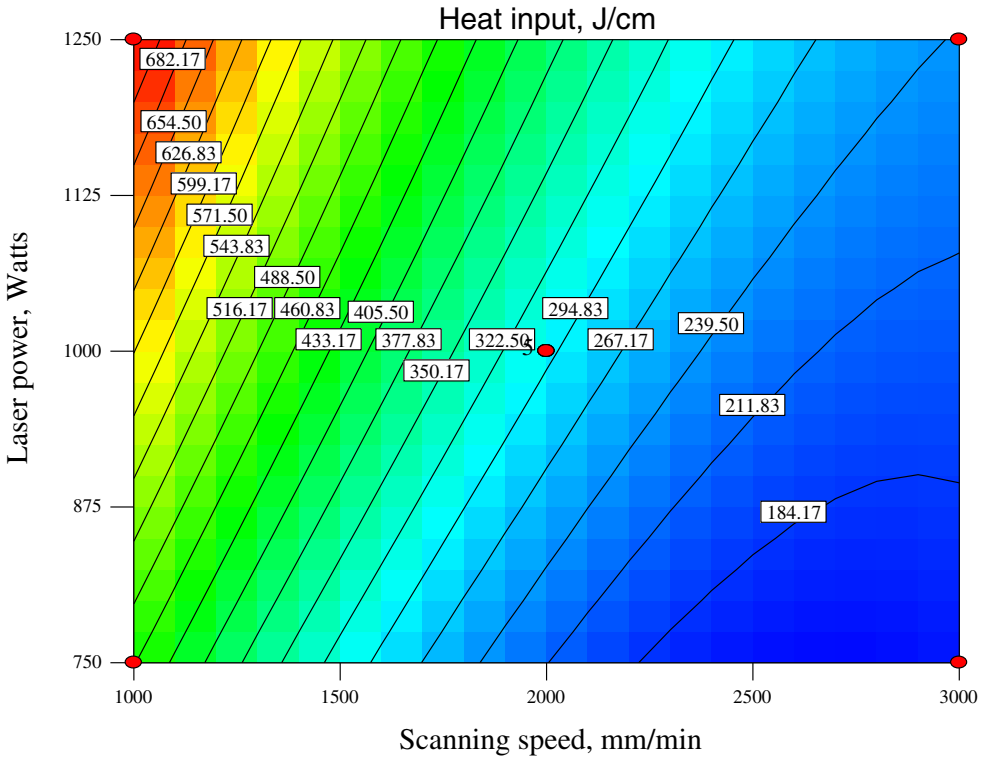


**Fig. 22** Contours graph shows the effect of LP and SS on the heat input

design as well as validation data, mean absolute percentage errors for ANN model are lower than as compared to RSM models. Considering the RMSE criterion of prediction accuracy, from the results and the Table 9, it has been observed that ANN models of HI and σ are predicted lower values of RMSE values of 0.0438 and 0.8099 for design data, and 0.00367 and 0.2349 for validation data as compared RSM models values 8.5749 and 1.0309 for design data, and 18.750 and 1.3919 for validation data, respectively. Thus, it is evident that for both design and validation data, the ANN model predicts more accurate results than the RSM model. Therefore, from the three criterions of validity, coefficient of determination (*R*-Squared), mean absolute error %, and RMSE, it can be concluded that the ANN model predicts more accurate and precise output results than the RSM model.

In order to test the accuracy of the prediction from the developed models, the experimental values were compared with predicted values of RSM and ANN models of HI and σ for all 17 experiments of design data. Figures 16 and 17 shows the comparisons of experimental values with predicted values

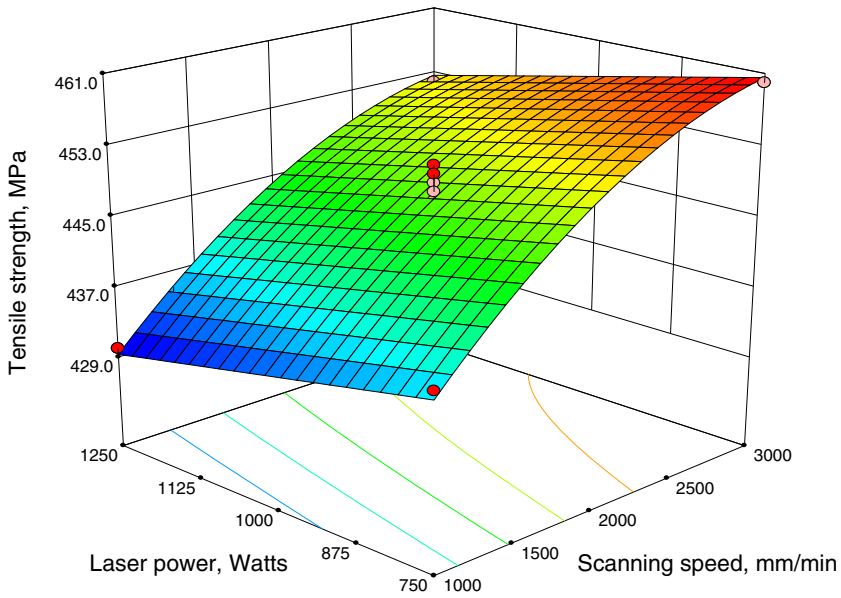


**Fig. 23** 3D graph shows the effect of LP and SS on the tensile strength

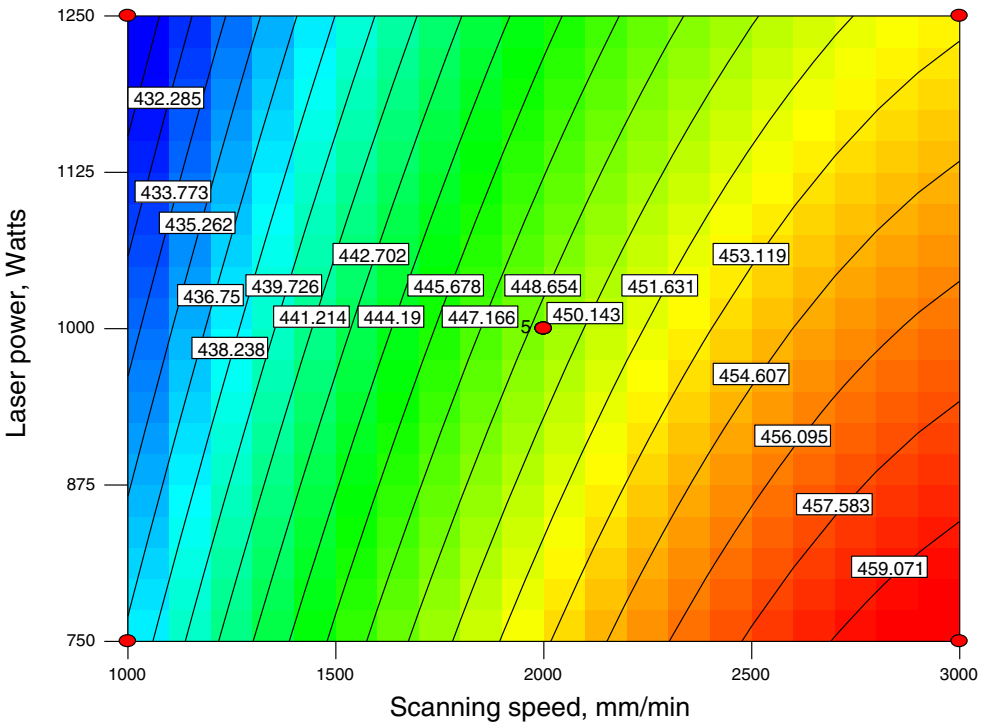


**Fig. 24** Contours graph shows the effect of LP and SS on the tensile strength

of RSM and ANN models of HI and σ, respectively. From the figures, it has been observed and ensured that predicted values of HI and σ for both RSM and ANN models are in close agreement with the experimental values.

## 4.6 Effect of heat input on tensile strength

Figure 18 shows the relationship between the σ and HI. This figure indicates that as heat input increases, tensile strength decreases. From the figure, it has been also observed that the higher values of σ are owing to low heat input and faster cooling rate. It may be noted that as cooling rate increases, relative elongation also increases and, hence, the higher the hardened tensile strength. Tensile strengths increase in the order of α and β microstructure with lower values of heat input, while elongation decreases in the order of coarse microstructure due to the increased heat input. Therefore, specimens of higher values of heat input encountered lower

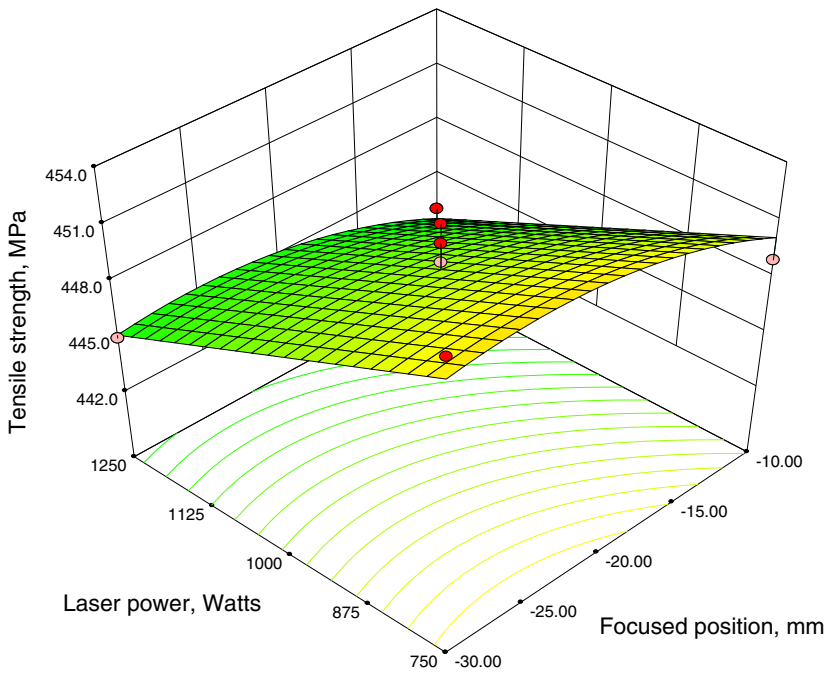


**Fig. 25** 3D graph shows the effect of LP and FP on the tensile strength

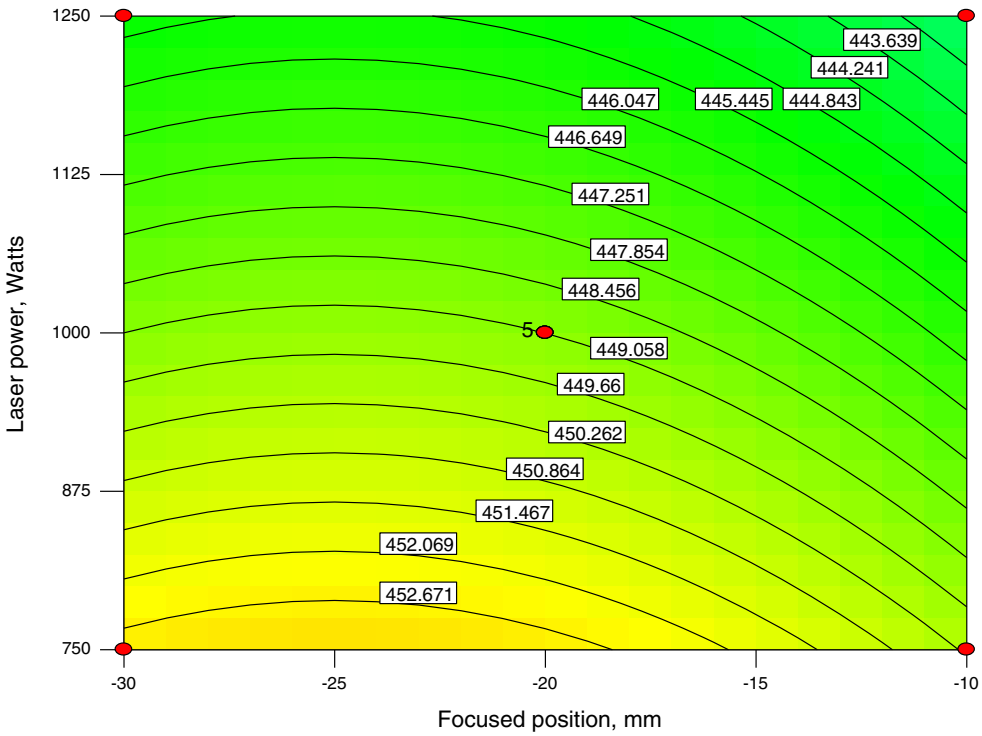


**Fig. 26** Contours graph shows the effect of LP and FP on the tensile strength

values of tensile strength. The lower range of heat input values with intermediate values of laser process variables, LP, SS, and FP ensured higher value of σ and achieved excellent grain formation and orientation of fine α and β phases. Also, the tensile strength increase can be attributed to solid-solution strengthening by the formation of titanium carbonitrides, titanium oxides, and titanium carbure that are also believed to be responsible for grain refinement [29].

Figures 19 and 20 show the microstructures of hardened or fusion zone, heat affected zone (HAZ) and base material for the two sets of laser process parameters, LP=750 W, SS=3,000 mm/min, FP=−20 mm with lower value of heat input 150 J/cm and LP=1,250 W, SS=1000 mm/min, FP=−20 mm with higher value of heat input 750 J/cm at ×200 magnification, respectively. The equiaxed grains appeared in the matrix. The laser-welded surfaces indicate typical casting structures composed of equiaxed grains in the centre and dendritic grains in the outside of the welded seam. The size of the grains for the higher heat input specimen is the largest, while the specimen with lower input is the smallest in the fusion zone as depicted by Figs. 19 and 20, respectively. The laser-hardened zone is clean. It has been seen that significant grain coarsening has occurred in the HAZ adjacent to the base material. The degree of grain coarsening increases as one moves to the fusion zone.

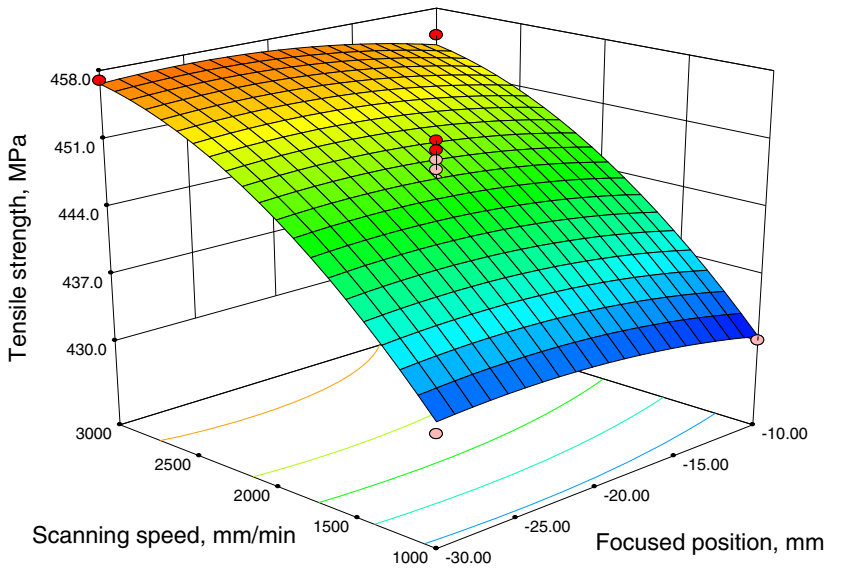


**Fig. 27** 3D graph shows the effect of SS and FP on the tensile strength

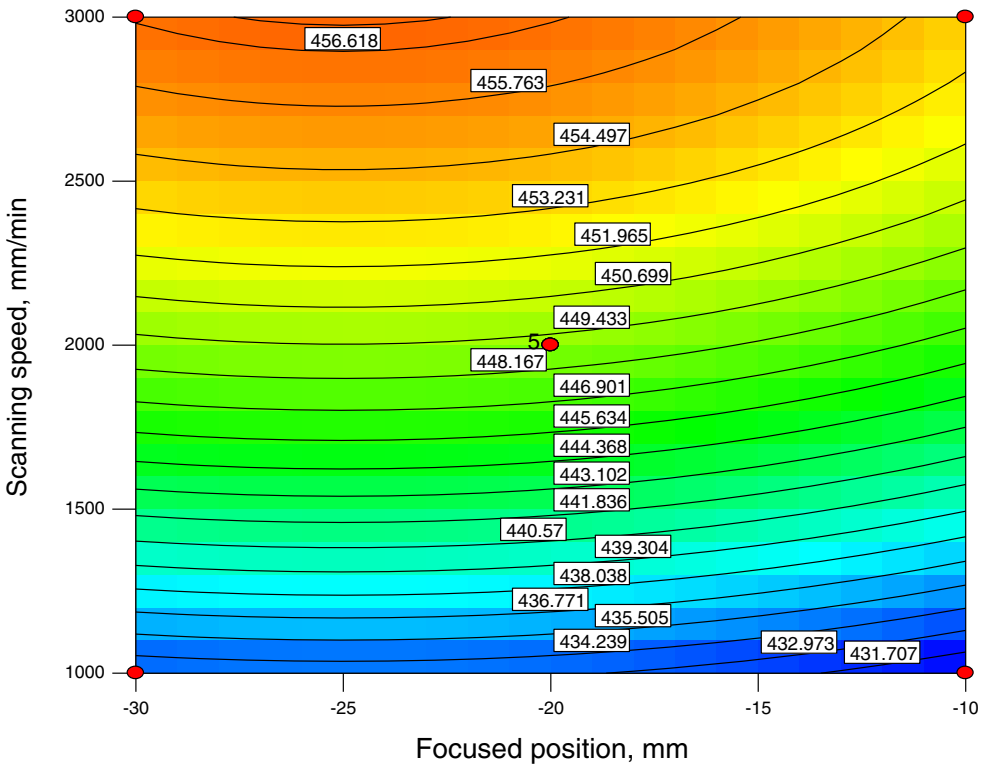


**Fig. 28** Contours graph shows the effect of SS and FP on the tensile strength

The HAZ undergoes strong thermal cycles involving rapid heating and cooling. Because the kinetics of the grain growth depends on temperature, the evaluation of the grain structure in the HAZ is different from isothermal processing of metals and alloys. Thus, decreasing the heat input provides a steeper distribution of peak temperatures in the HAZ, and thereby increase in tensile strength has been encountered. Increasing the heat input increases the width of the HAZ and time of exposure to temperatures and reduces the cooling rate [30]. Therefore, it is evident from Fig. 18 that as input increases, tensile strength decreases.

### 4.7 Effect of process factors on heat input and tensile strength

#### *4.7.1 Heat input*

The laser HI is directly related to the LP and SS. It can be calculated directly from the HI = LP/SS. The reason of predicting the heat input is to develop a model to include it into optimum step in future work and to predict the effect of it on the tensile strength importantly. From Figs. 21 and 22, it is evident that as LP increases and SS decreases, the heat input increases.

#### *4.7.2 Tensile strength*

From the results in Table, it is studied that those parameters significantly affecting the σ are LP and SS. The most influencing factor is SS. Effect of FP on tensile strength is significant but it has less influence as compared to LP and SS. From Figs. 23 and 24, it is seen that tensile strength increases considerably as SS increases and decreases marginally as LP increases. Since heat input is directly proportional to LP and inversely proportional to SS, as heat input increases, tensile strength decreases. Therefore, from the figures, it is evident that tensile strength increases with decrease in LP and increase in SS thereby decreasing in heat input.

Figures 25 and 26 indicate that as LP decreases and FP decreases (i.e., from −10 to −30 mm FP) the tensile strength increases. It is also observed from Figs. 27 and 28, and it is evident that as SS increases, tensile strength increases considerably and increases marginally as FP decreases (i.e., from −10 to −30 mm). From the above results, it is confirmed that tensile strength showed higher values at focused position −30 mm as compared to FP at −10 and −20 mm means that as the defocusing increases heat input decreases and hence the tensile strength increases marginally.

## 5 Conclusions

This paper has illustrated the use of design of experiments for conducting experiments. Two models were developed for predicting the heat input and tensile strength of laser-hardened unalloyed titanium using RSM and ANN. This

paper also described the effect of laser process parameters on heat input and tensile strength of laser-hardened commercially pure titanium and evaluated the comparison of the heat input and tensile strength predictive models based on ANN and RSM. From these investigations, the following important conclusions are derived:

1. Box–Behnken design can be employed to develop mathematical models for predicting laser hardened-bead geometry.
2. The desired heat input and tensile strength with high quality of LTH can be achieved by choosing the working condition using the developed models.
3. Heat input plays an important role in deciding the tensile strength of the laser-hardened commercially pure titanium material. It is investigated that, in case of LTH though, as scanning speed increases, heat input decreases and vice-versa. Conversely, as laser power increases heat input increases and vice-versa. Therefore, both scanning speed and laser power have positive effect on all the responses investigated.
4. Bead width as well as depth of hardening linearly decreases with increasing scanning speed. It is evident that the heat input provides a useful tool to manipulate the tensile strength. It is clearly observed that the heat input linearly increases with increase in laser power and decrease in scanning speed.
5. It has been found that a trend of increased tensile strength with the decrease of hardening heat input and a trend of increased tensile strength with the increase of hardening cooling rate. As heat input decreases, there will be faster cooling rate. Considering the effect of HI on σ, it was found that the lower the heat input, the faster the cooling rate. Tensile strength increases with decrease in laser power and increase in scanning speed with defocused beam, i.e., with higher beam spot size (from −10 to −30 mm FP).
6. RSM and ANN models were developed based on experimental data to predict the relationship between the laser hardening process variables (LP, SS, and FP) and heat input and tensile strength parameters.
7. Artificial neural networks are a powerful tool for modeling of laser transformation hardening of titanium and its alloys. ANN models performed better than the RSM models in describing the laser transformation hardening process parameters LP, SS, and FP, and characteristics of the hardened-bead profile parameters such as heat input and tensile strength characteristics. The predictive ANN model is found to be capable of better predictions of HI and σ. The results of the ANN model indicate it is much more robust and accurate in estimating the values of heat input and tensile strength parameters when compared with the RSM model.

**Acknowledgments** The authors are grateful to management of welding Research Institute, BHEL, Tiruchirappalli- 620 014, Tamil Nadu, India for extending the facilities of Laser Materials Processing Laboratory to carryout the research work in the area of laser materials processing. The authors also wish to express their sincere thanks for the constant encouragement received from the faculties of MANIT Bhopal during the course of work.

## References

1. Steen WM (1991) Laser Material Processing. Springer, London
2. Tam KF, Cheng FT, Man HC (2002) Enhancement of cavitation erosion and corrosion resistance of brass by laser surface alloying with Ni–Cr–Si–B. Surf CoatTechnol 149:36–44
3. Katsamas AI, Haidemenopoulos GN (2001) Laser beam carburizing of low-alloy steels. Surf CoatTechnol 139:183–191
4. Cheng Man FT, Man HC (2003) Laser transformation hardening of AISI 440C martensitic stainless steel for higher cavitation erosion resistance. Surf CoatTechnol 173:96–104
5. Annadurai G, Ling LY, Lee JF (2008) Statistical optimization of medium components and growth conditions by response surface methodology to enhance phenol degradation by *Pseudomonas putida*. J Hazar Mate 151:171–178
6. Box GEP, Behnken DW (1960) Some new three level designs for the study of quantitative variables. Technimotrics 2:455–475
7. Evans M (2003) Optimisation of manufacturing processes: a response surface approach, Carlton House Terrace London
8. Kannan N, Rajakumar A, Rengasamy G (2004) Optimisation of process parameters for adsorption of metal ions on straw carbon by using response surface methodology. Environ Technol 25:513–522
9. Rana P, Mohan N, Rajagopal C (2004) Electrochemical removal of chromium from wastewater by using carbon aerogel electrodes. Water Res 38:2811–2820
10. Annadurai G, Sung SS, Lee DJ (2004) Optimization of floc characteristics for treatment of highly turbid water. Sep Sci Technol 39:19–42
11. Deeng KD, Mohamed AR, Bhatia S (2004) Process optimization studies of structured Cu–ZSM-5 zeolite catalyst for the removal of NO using design of experiments (DOE). Chem Eng J 103:147–157
12. Levision KK, Takayama K, Isowa K, Okaba K, Nagai T (1994) Formulation optimization of indomethacin gels containing a combination of three kinds of cyclic montoterpenes as percutaneous penetration enhances. J Pharm Sci 83:1367–1372
13. Shirakura O, Yamada M, Hashimoto M, Ishimaru S, Takayama K, Nagai T (1991) Particle size design using computer optimization technique. Drug Dev Ind Pharm 17:471–483
14. Montgomery DC Design and data analysis of experiments, 5th edn. John Wiley & sons, New York Inc. 1997, 2001
15. Khuri AI, Cornell JA (1996) Response surfaces design and analysis, 2nd edn. Marcel Dekker, New York
16. Box GEP, Behnken DW (1960) Some new three level designs for the study of quantitative variables. Technometrics 2:455–475
17. Perzyk M, Kochanski AW (2001) Prediction of ductile cast iron quality by artificial neural networks. J Mater Process Tech 109:305–307
18. Rafiq MY, Bugmann G, Easterbrook DJ (2001) Neural network design for engineering applications. Comput Struct 79:1541–1552
19. Kenig S, Ben-David A, Omer M, Sadeh A (2001) Control of properties in injection molding by neural networks. Eng Appl Artif Intel 4:819–823
20. Limpon RP (1987) An introduction to computing with neural nets. IEEE ASSP Magazine 4–22
21. Nielsen RH (1998) Neurocomputing picking the human brain. IEEE Spectrum 25(3):36–41

22. Fausett F (1994) Fundamentals of neural networks: architectures, algorithms and applications. Englewood Clis., NJ, USA, pp 155–178
23. Haykin S (1994) Neural networks, a comprehensive foundation. McMillian College Publishing Company, New York, pp 198–203
24. Avci E, Turkoglu I, Poyraz M (2005) Intelligent target recognition on based wavelet packet neural network. Elsevier Expert Syst Appl 29:175–182
25. Avci E, Turkoglu I, Poyraz M (2005) Intelligent target recognition based on wavelet adaptive network based fuzzy inference system. Lecture notes in computer science 3522 Springer-Verlag, pp 594–601
26. Wong BK, Bodnovich TA, Selvi Y (1997) Neural network applications in business: a review and analysis of the literature. 1988–1995. Decis Support Syst 19:301–320
27. Minitab User's Guide 2: Data analysis and quality tools. Minitab Inc., 2000
28. Erb RJ (1993) Introduction to backpropagation neural network computation. Pharm Res 10:165–170
29. Mohandas T, Madhusudhan Reddy G, Naveed MA (1999) Comparative evaluation of gas tungsten and shield metal arc welds of a ferritic stainless steel. J Mater Process Technol 94(2/3):133–140
30. Adams CM Jr (1976) Heat flow in welding. In: Weisman A (ed) Welding handbook, Vol.1, 7th edn. AWS, Miami, p 80